# Dynamic Economic Dispatch using a Hybrid Neural Network with Resource-aware Scenario Selection

Joshua Darville
University of Miami
1320 South Dixie Highway
Coral Gables, FL 33146, USA
jmd437@maimi.edu


Jin Curia
University of Miami
1320 South Dixie Highway
Coral Gables, FL 33146, USA
jxc2264@miami.edu

Nurcin Celik*
University of Miami
1320 South Dixie Highway
Coral Gables, FL 33146, USA
celik@miami.edu

*Corresponding Author

**Abstract –** Modern large-scale power systems continue to increase in complexity, uncertainty, and the dimensionality of the sensory data. Thus, traditional solution methods are being outpaced by an evolving problem and often meet their limitations when used at scale. Adaptive solutions that can evolve in tandem with the problem are required to solve the complex, sequential decisions of large-scale power systems. Data-driven methods found in machine learning provide an adaptive solution for microgrid (MG) technology and are being investigated for their utility in this field. Hence, we propose a modular framework for the offline development of these complex models and their utility for online decision-making. In this framework, the proposed smart scenario selection (SSS) algorithm reduces high dimensional data to the most diverse states. A multi-objective dispatch policy was used to obtain an exact solution for the most diverse states. The epsilon constraint method was used to derive the Pareto frontier for each state and decision criteria was used to determine the best-compromise solution. The state space and solution space were then merged into datasets for the IEEE-18 and IEEE-33 test networks, respectively. Neural networks (NNs) were trained using these datasets to scale the predictive performance of traditional solution methods for real-time dispatch across both test networks. The results show the SSS algorithm significantly reduces the state space and consequently the overall offline development time. Furthermore, the NNs' showed stable learning without overfitting and the architecture varies with the resources from each test network.

# 1 INTRODUCTION

Energy surety remains the primary concern for many countries. In the wake of existing factors such as the rising global population, high frequency of natural disasters, and accelerating climate change due to carbon emissions ($CO_2$), the use of distributed energy resources (DERs) into existing grid technology is essential to sustain the global population. Microgrids (MGs) are evolved power distribution networks that efficiently allocate energy from the DERs within their networks to satisfy both retail and wholesale energy demand [1]–[3]. Furthermore, MGs ensure the reliability of energy distribution and faster response times to faults than their traditional counterparts. These self-healing capabilities improve the MG's robustness for all its agents, including the energy producers, consumers, and transmission system operators.

The caveats to the benefits of MG integration are the issues posed by large scale data flow among all its agents and the stochastic nature of renewable power generation [4]. These issues include the need for i) a reduced order model that captures the MG system behavior and adheres to the physics equations governing power systems [5] (eg. electrical power flow and frequency regulation); ii) an accurate method of forecasting both the external climate data and internal market data, to mitigate the impact uncertainty on the dispatch decisions; iii) decision criteria for the near- or global-optimal dispatch decisions from the ensemble of solutions (Pareto Front) generated by multiple objectives within the MG dispatch model; iv) and a method of reducing the computational burden incurred from large-scale sequential decision-making. Hence, future power systems will require MGs to monitor localized energy production and make the appropriate decisions to sustain the overall grid stability.

## 1.1 Modeling Physical Systems

To address the first issue, an appropriate modeling approach should be used for MG systems. Analytical models, simulations, and empirical experiments are approaches employed to model the behavior of a physical system under various scenarios ranging from the most to least abstract approach. The degree of abstraction of the modeling approach is inversely proportional to its development cost, where analytical models are the most abstract but cheapest to develop. Moreover, the model can be either deterministic where all information is known, or stochastic where parameter uncertainty is introduced over the planning horizon.

In the case of MG operational planning, optimization models are used to represent sequential dispatch decisions made by the MG throughout the day. Since it is often infeasible to extract a closed-form model of a MG, the optimization models are simulated for a specific scenario. The simulated results and the modeling assumptions can be considered valid after enough replications. Dynamic data-driven application systems (DDDAS) is a powerful paradigm first introduced by [6] which facilitates the performance of a simulation through the symbiotic relationship with the physical system. DDDAS enables an application-specific framework to ascertain how the system and environmental data should be harvested from the MG system as the data is streamed to the MG simulation. DDDAS has experienced success across a spectrum of fields including cloud-data access [7]–[10], materials and cybersecurity and smart cities [11]–[14], flight paths and aerospace design [15]–[19], and smart grid optimization [20], [21]. Although the DDDAS provides a foundational template for the integration of various modules within an application-specific framework, the individual modules require state estimation [22], [23] and fidelity selection techniques [24]. In this study, the proposed smart scenario selection (SSS) method is used to reduce the dimensions of the MG's system state space based on historical data. Moreover, solution methods are required for modeling complex problems such as bulk power systems.

Complex power system models are typically solved with convex optimization methods, programming methods, and heuristic methods. Convex optimization methods have rigorous mathematics that provide an exact solution. However, these methods are often used for low dimensional data in deterministic models and require an explicit objective function which is difficult to abstract from the real-world scenarios of a MG system. Programming methods such as mixed integer programming, dynamic programming, and stochastic programming can solve stochastic models for near optimal solutions [25]. However, these methods also require convex objective functions and must recalculate for each scenario of the problem. Thus, available computational resources limit the scalability of these methods for decision-making in some scenarios. Similarly, non-convex objective functions are often observed in physical systems where there are multiple objectives. Heuristic methods can also be used to solve deterministic and stochastic models with non-convex objective functions [26]. However, these methods obtain a near optimal with a certain probability but can theoretically obtain an exact solution with infinite time. Although these methods are scalable, they are less robust than the previous solution methods. Thus, heuristic solutions may vary under uncertainty despite convergence.

## 1.2   Proposed Modeling Approach

Researchers have made significant progress across the fields of Machine Learning (ML), seeking to develop an all-purpose solution method for physical systems. This progress has resulted in the emergence of mature, vetted ML algorithms. Artificial Neural Networks (NNs) are a subset of ML, typically referred to as Deep Learning. Neurons are the fundamental units of NNs which are interconnected through layers, performing calculations on their inputs, and propagating them forward. Optimization algorithms and a loss function are used to calculate an error value which is backpropagated through the network to improve its prediction rate. The repetition of that process is what is referred to as training and learning. NNs have been used to approximate non-linear objective functions [27], to forecast consumption data for demand response policies [16], and for post-processing to enhance existing dispatch solutions [17].

In this study, the task of finding the ideal MG dispatch decisions at scales is addressed by mapping from the state space to the solution space using NNs. NNs are capable of accurately approximating functions between two vector spaces by only observing a subset of all possible mappings. This trait distinguishes them from the trivial exhaustive search approaches. Thus, the problem becomes selecting a suitable subset of the state space to train the NN and approximate the transition function between both domains in an accurate and robust manner. The criteria and methods for selecting a suitable subset of the MG state space are captured in the SSS algorithm. By strategically selecting states with SSS in conjunction with the mapping of a NN, this complete method offers an adaptive alternative to current dispatch policies and solution methods.

NNs have many advantages compared to traditional solution methods. They do not require an objective function to be convex or explicitly defined compared to convex optimization methods. Moreover, this solution makes decisions according to the current state in real-time and does not require the solver to restart like programming methods. Unlike convex optimization and programming methods, NNs can handle higher dimensional data like heuristic methods. However, NNs are more robust than most heuristics and can stably learn from historical data. A robust model is critical for reliable predictions and the overall resiliency of MG operations given a previously unseen state. Paramount to the lack of deficiencies observed by the previous solution methods, NNs implicitly detect complex nonlinear relationships between the dependent and independent variables. The disadvantages of NNs include their "black box" nature when justifying the results obtained, the

great computational burden incurred during offline training, and a proclivity to overfit where regularization is required to discourage unnecessary model complexity. The advantage and disadvantages of the solution methods are described in Table 1.

Table 1: Advantage and disadvantages of solution methods used to solve MG models.

| Solution Method | Advantages | Disadvantages |
|---|---|---|
| Convex Optimization | - has rigorous mathematics<br>- obtains an exact solution | - used for low dimensional data<br>- requires a convex objective<br>- does not apply to stochastic models |
| Programming Methods | - obtain an exact solution<br>- can handle high dimensional data<br>- apply to both deterministic and stochastic models | - require a convex objective<br>- have limited scalability |
| Heuristics | - obtain a sufficient local optimum<br>- do not require a convex objective<br>- can handle high dimensional data<br>- apply to both deterministic and stochastic models | - require infinite time for an exact solution<br>- are less robust than other solution methods<br>- scalability can vary |
| Neural Networks | - are both the model and solution<br>- can handle high dimensional data<br>- do not require a convex objective<br>- are scalable for most scenarios<br>- can be more robust than other heuristics | - determining the appropriate architecture<br>- require existing solutions for training<br>- interpretability |

This paper presents the use of a NN to predict the dispatch decisions of a MG system using solutions from existing dispatch policies. The proposed framework integrates the advantages of existing programming methods to compensate for the deficiencies observed in NNs since NNs inherently compensate for the disadvantages of existing programming methods. The proposed framework for MG dispatch uses the symbiotic concept from the DDDAS paradigm as a tertiary control scheme for large-scale, bulk power systems. Hence, this study contributes:
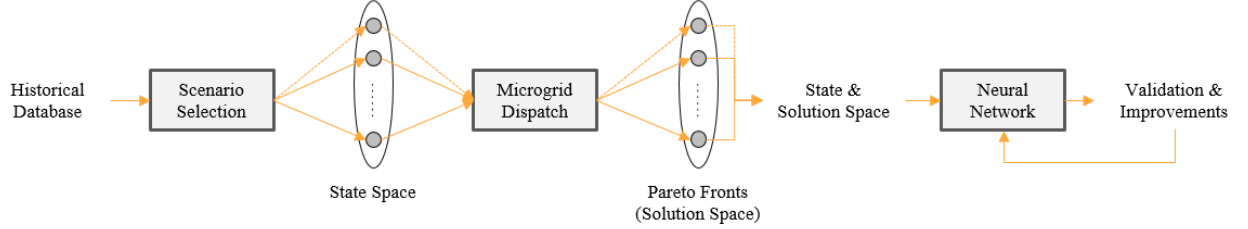
- A modular MG dispatch framework for offline modeling and online decision-making, by using existing dispatch policies to supervise deep learning.
- A general method of fidelity selection using a probabilistic variate of full factorial design; this assumes the treatments reflect the scenarios experienced by the MG system.
- A scalable and generalized design for a neural network that can learn MG system data and adapt to demand-side management (DSM) practices

This article is presented in subsequent sections. Section 1 provided an overview of the problem and its consequent challenges posed to the research community, the various methods used to model and solve the problem while highlighting their tradeoffs, and the proposed solution to the problem and its contributions. Section 2 highlights the proposed MG dispatch framework for offline model development and online decision-making. Section 3 outlines the proposed SSS method for selecting the most diverse and likely states. Section 4 describes the dispatch policy used along with its solution methods and decision criteria. Section 5 discusses the results of the proposed SSS algorithm, the NN's architecture, hyperparameters, and performance. Finally, Section 6 concludes the findings of this study.

## 2 MICROGRID DISPATCH FRAMEWORK

The proposed framework can be divided into two phases. The first phase illustrates the offline development of NNs for predicting MG dispatch decisions while the second phase illustrates the integration of NNs for online dispatch.

**Offline Development**



**Figure 1:** Framework for MG dispatch using NNs with SSS.

During the offline development phase in Figure 1, independent modules are tailored in series to develop the NN. Initially, climate data (external data) is collected from [28] from June 2019 to July 2020. This external data is fed to the proposed SSS algorithm to isolate the best representative days (states) which indicate unique climate behavior. This state estimation technique selects the states throughout the year (state space) describing the overall climate behavior while preserving most of the external data. A comprehensive MG dispatch policy based on [29] is used to acquire an exact solution for each state. The MG dispatch policy is a multi-objective, mix integer programming formulation and generates a Pareto frontier for the conflicting objectives in each state. Decision criterion is used to determine the best-compromise (solution) in each Pareto frontier throughout the set of Pareto fronts (solution space). The solutions from the MG dispatch policy are merged with the states from the SSS algorithm into a new dataset (state and solution space) for training the proposed NN. Since the NN's learning mechanism allows for both multi-output classification and regression, it is uniquely positioned compared to other machine learning algorithms for mapping the state space of a physical system to its solution space. Thus, various data types can be conveyed by the resulting prediction, unlike most machine learning methods.

**Online Application**
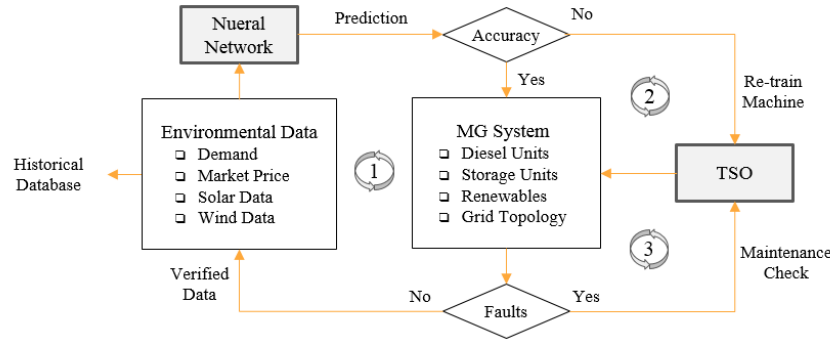


**Figure 2:** Framework for MG dispatch using NNs with SSS.

During the online phase of Figure 2, the NN developed in the first phase is used to predict dispatch decisions. The online phase can be described via 3 cycles. In cycle 1, the fault-free data from the MG system is fed to the neural network to predict the appropriate dispatch decisions and is simultaneously stored in a historical database. Otherwise, if the resource data (internal data) from the MG system indicates faulty equipment, the transmission system operator (TSO) would be

notified in cycle 3 to schedule a maintenance check. Likewise, if the NN's accuracy does not satisfy a threshold set by the TSO, the TSO would be notified in cycle 2 that the NN needs to be re-trained using the current state and solution space.

Cycle 2 highlights a limiting factor for artificial intelligence (AI) models as data is accumulated; current information may vary significantly from previous information. The SSS algorithm would determine whether this is due to outliers or is a sustain behavior and should be considered a new state. Regardless of the determination, the AI model must be re-trained using the data accumulated since its previous deployment. As the data scales, the required training time for most AI models increases and this limits their utility in physical systems. However, NNs require large amounts of data to observe variation during training and can handle the curse of dimensionality when used at scale. Thus, the predictive performance should improve with each re-deployment of the NN, providing a robust, adaptive solution for physical systems.

## 3   SMART SCENARIO SELECTION

Each modeling approach including analytical, simulation and empirical experiments, has its unique taxonomy describing aspects of their modeling approach. Although the terminology differs, the jargon is analogous across all approaches. The analogous taxonomy used across modeling is outlined in Table 2 and are used interchangeably throughout this study.

Table 2: Analogous terminology across various modeling approaches.

| Analytical | Simulation | Empirical Experiments |
|---|---|---|
| Parameters | Input | Factors |
| Objective Function | Output | Response |
| Scenario | Replication | Treatments |
| Sensitivity | Fidelity | Levels |
| Optimality Gap | Confidence Interval | Risk |

The SSS algorithm combines the accuracy of an empirical experiment with the cost-effectiveness of an analytical model to reduce the scale of the analytical model and preserve most of the empirical data. Among the design types for planning and conducting experiments, the full factorial design is the most conservative design type. The full factorial design supports both continuous and categorical factors with arbitrary numbers of levels, where scenarios are assumed to be randomized [30]. This technique provides a discrete number of treatments for every factor-level combination, which outlines the model's state space as previously depicted in Figure 1. The underlying assumption of the SSS algorithm is the treatments of an experimental design are equivalent to the scenarios denoting the state space of an analytical model. The methodology for the proposed scenario selection technique is described in Table 3.

Table 3: Smart Scenario Selection Algorithm

**Input**: $n$ input vectors from external climate factors, threshold $\alpha$

1. use $n$ factors to approximate the power signals
2. obtain the probability density functions for $n$ factors
3. select a box plot configuration to model the desired sensitivity
4. assign levels to each factor equivalent to its number of quartiles
5. obtain all possible scenarios according to a full factorial design
6. assign the joint probability to each scenario
7. remove scenarios where the state was not observed in the dataset
8. filter dataset to locate days with the highest frequency of each scenario

9.  filter states according to $\alpha$ for the most significant scenarios
    **Output:** Significant scenarios dominating the state space

---

The number of replications required to experiment increases exponentially with the number of factors when using a full factorial design. Although the empirical experiment does not scale, the SSS algorithm address this issue. The SSS algorithm limits the factors to the external data and the levels are not arbitrarily defined as seen in a traditional full factorial design. The factors are instead derived from the external data which cannot be regulated with DSM policies, unlike those derived from the internal data. The scenarios generated by the SSS algorithm are based on uncertain factors while known parameters are assumed to have a constant effect on MG dispatch. Furthermore, the levels are determined based on the desired sensitivity of the model and are obtained from the quartiles of each factor's box plot. After identifying the uncertain factors and a box plot configuration base on the desired sensitivity, the design table of treatments is generated according to a full factorial design. Each factor's best-fit distribution is obtained to determine the likelihood of each treatment throughout the experiment. Thus, the SSS algorithm isolates significant scenarios according to a pre-defined threshold of the likelihood of observing that treatment throughout the experiment. Outlier detection is used to refine the scenario set generated from the experimental design with a threshold $(\alpha)$ such that $(P(factor \mid level\ x) < \alpha)$ indicates an unlikely scenario derived from outliers. To verify the portion of the state space covered by the significant scenarios, probability theory states the probability of simultaneously occurring event can be calculated such that $(a \cap b) = P(a) * P(b)$. Thus, the sum of all treatment combinations (scenarios) deemed significant should approximately equal to 1. Consequently, the experiment's state space is reduced while most of the factors' information is retained. Thus, the SSS algorithm adapts a traditional full factorial design to more large-scale problems where it would otherwise be an infeasible approach.

## 3.1  Factor Approximations & Distribution

Initially, sensory data from the historical database is used to approximate the power signals from the DERs and their best-fit distributions are determined using the squared error (SE). The sensor data includes uncertain factors such as load, market price, ambient temperature, solar irradiance, and wind speed.

$$F_t \sim N(\mu_t, \sigma)\ \ where\ \mu = PD \times PF_t\ and\ \sigma = 0.05\mu \tag{1}$$

The uncertainty of the forecasted hourly load demand $(D_t)$ is modeled in (1) as a function of peak demand $(PD)$ and the power factor $(PF_t)$. It assumed the loads are relatively close to the DERs in a localized distribution network and a power factor of 1 is applicable. A Gaussian distribution is assumed to reflect the load uncertainty with a 5% standard deviation used [31], [32].

$$f(x;\ \mu, \lambda) = \left[\frac{\lambda}{2\pi x^3}\right]^{1/2} exp\left(\frac{-\lambda(x - \mu)^2}{2\mu^2 x}\right) \tag{2}$$

The market price of electricity for an entire month is considered in (2) assuming the monthly price follows a similar pattern throughout the year. An Inverse Gaussian was used by [29] as the best fit to reflect the prices obtained from [33], where the average monthly rate ($\mu$) is 10.57 cents/kWh.

$$PV_t = FF \cdot V_t \cdot I_t \qquad (3)$$

$$V_t = V_{oc} - k_v[T_t^{cell} - 25] \qquad (4)$$

$$I_t = SI_t \cdot (I_{sc} + k_i[T_t^{cell} - 25]) \qquad (5)$$

$$T_t^{cell} = T_t^{amb} + \frac{(T^{nom} - 20)}{0.8} \cdot SI_t \qquad (6)$$

$$f(x = T_t^{amb}; \mu, \sigma) = \frac{1}{\sqrt{2\pi\sigma^2}} exp^{-\frac{1}{2}\left(\frac{x-\mu}{\sigma}\right)^2} \qquad (7)$$

$$f(x = SI_t) = \frac{\Gamma(\alpha + \beta)}{\Gamma(\alpha)\Gamma(\beta)} x^{\alpha-1}(1 - x)^{\beta-1} \qquad (8)$$

$$\mu = \frac{\alpha}{\alpha + \beta} \qquad (9)$$

$$\sigma^2 = \frac{\alpha\beta}{(\alpha + \beta)^2(\alpha + \beta + 1)} \qquad (10)$$

The power signal for solar generation is modeled in (3)-(6). The hourly power output from solar panels ($PV_t$) is the function of a constant fill factor ($FF$) related to the panel characteristics along with voltage ($V_t$) and current ($I_t$). Similarly, solar irradiance ($SI_t$), nominal cell ($T^{nom}$) and ambient temperature ($T_t^{amb}$) data are collected by sensors to calculate the cell temperature ($T_t^{cell}$). The voltage and current coefficients ($k_v, k_i$) along with the open-circuit voltage and short circuit current ($V_{oc}, I_{sc}$) depend on the solar panel attributes from the manufacturer. $T_t^{amb}$ follows a normal distribution in (7) where $\mu$ = 77.54 and $\sigma$ = 7.54 with a SE of 0.004. However, $SI_t$ follows a beta distribution in (8) where the gamma function ($\Gamma$) is denoted with auxiliary variables ($\alpha, \beta$) in (9)-(10). The beta function is defined such that $\alpha$ = 0.735 and $\beta$ = 2.55 with an SE of 0.00002.

$$PW_t = \begin{cases} P_w \times \dfrac{v_t^w - v_{ci}}{v_r - v_{ci}} & if \ v_{ci} \leq v_t^w \leq v_r \\ P_w & if \ v_r \leq v_t^w < v_{co} \\ 0 & else \end{cases} \qquad (11)$$

$$f(x = v_t^w; \alpha, \beta) = \frac{x^{\alpha-1}}{\beta^\alpha \Gamma(\alpha)} exp^{\left(-\frac{x}{\beta}\right)} \qquad (12)$$

$$\alpha = \frac{\mu^2}{\sigma^2} \qquad (13)$$

$$\beta = \frac{\sigma^2}{\mu} \qquad (14)$$

The hourly power output from wind turbines $PW_t$ is modeled in (11) by a piecewise function of the wind speed ($v_t^w$) at the site and the rated power ($P_w$). The power performance curve of a wind turbine is sectioned by the cut-in speed ($v_{ci}$), cut-out speed ($v_{co}$) and rated speed ($v_r$) to determine the total power generated. $v_t^w$ follows a gamma distribution in (12) and is denoted with auxiliary

variables $(\alpha, \beta)$ in (13)-(14). The gamma function is defined such that $\alpha = 1.21$ and $\beta = 7$ with an SE of 0.019. Similar distributions were obtained for long-term sensory data such as solar irradiance and wind speed by [34] and [35], respectively. After the power signals and likelihood functions were obtained for each factor in (1)-(14), the levels need to be determined to generate the final design table.

## 3.2  Level Selection

The design table of treatments is derived from each factor and the factor's levels are based on the chosen box plot configuration to model the physical system. The various box plot configurations allow for a tunable sensitivity of the simulation, and subsequently the levels of each external factor. Common box plot configurations are illustrated in Figure 3.
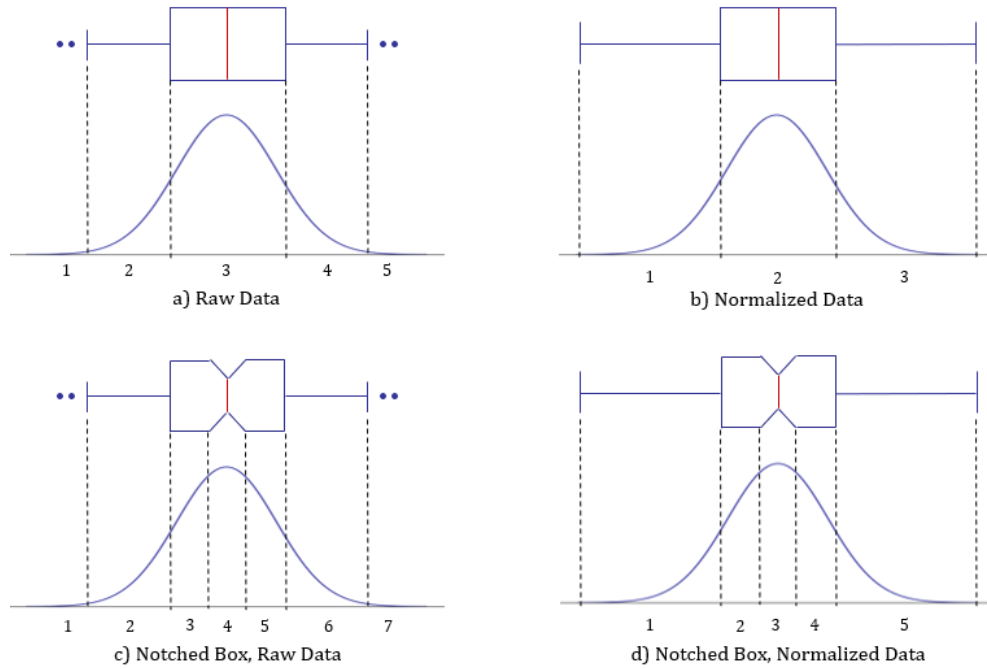


**Figure 3:** Box plot configurations for level selection

The box plot configuration influences the speed and accuracy tradeoff as the sensitivity increases with the number of levels, and consequently the model complexity with the number of resulting scenarios. Notably, quartiles on both sides of the whiskers are considered levels to ensure all data is used even if outliers are present. The number of quartiles (levels) across the box plot configurations in Figure 3 are [3, 5, 7], where the sensitivity of the model is directly proportional to the number of levels. After a box plot configuration is selected, the bounds segmenting the quartiles are used for integration along with each factor's probability density function (PDF). In the case of MG dispatch, the normalized data configuration would be appropriate if one is interested in a low sensitivity model of the macroclimate behavior where there is little focus on extreme climate events. Conversely, the notched box, raw data configuration should be selected if one is interested in the microclimate behavior throughout the state space. However, the raw data box plot configuration was chosen to isolate the scenarios or states based on outliers. Although this configuration includes states reflecting extreme climate events, it is less refined than the notched box, raw data

configuration and subsequently saves computational resources with a low sensitivity model. The raw data box plot configuration and the PDF for each factor were used to synthesize a design table where a probability is assigned to each scenario to isolate the most probable states. Moreover, the power signals for each state were fed to an existing dispatch policy to determine an exact solution for the most probable states.

## 4    MICROGRID DISPATCH POLICY

As previously illustrated in Figure 1, the dispatch decisions for each significant scenario are obtained using a modified dispatch policy based on [29]. The proposed dispatch policy provides an extension for frequency regulation and is termed the frequency emission dispatch (FED) model. This model was used in similar DDDAS based frameworks such as [24]. The best representative days derived using the SSS algorithm are input for this multi-objective model to obtain i) an exact solution for each significant scenario and ii) the Pareto Frontier derived from the conflicting objectives.

### 4.1    Dispatch Model Formulation

The FED model minimizes the total operational cost and $CO_2$ emissions which are quadratic functions. An upper linear approximation was used in this study to linearize the quadratic objectives for tractability purposes. The indices used throughout the FED model include buss $l \in \{1, \dots, L\}$, diesel unit $i \in \{1, \dots, I\}$, hour $t \in \{1, \dots, 24\}$, step $n \in \{1, \dots N\}$ and segment $k \in \{1, \dots, K\}$.

$$min \sum_{t=1}^{24} \sum_{l=1}^{L} \sum_{i=1}^{I} \sum_{k=1}^{K} \begin{bmatrix} x_{lt}RI_{lt} + u_{it}^k\, CI_i + g_{it}^k CS_i + v_t U^{min} + b_t U^{rt} \\ +u_{it}^k\, CU_i + \left(1 - u_{it}^k\right) CD_i \end{bmatrix} \tag{15}$$

$$min \sum_{t=1}^{24} \sum_{i=1}^{I} \sum_{k=1}^{K} u_{it}^k\, EI_i + g_{it}^k\, ES_i^k \tag{16}$$

Objectives: The first objective function (15) minimizes the total MG operational cost including the cost of interruption, the diesel unit operating cost, the MG's startup and shut down cost along with the cost of electricity bought from the main grid. In (15), $x_{lt}$ is the amount of interrupted load at a rate of $RI_{lt}$; $u_{jt}^k$ is a binary indicator of the diesel unit's status with an intercept of $CI_i$; $g_{jt}^k$ is the amount of power from the diesel unit that can be ramped at a slope of $CS_i$; $v_t$ is a binary indicator for connection to the main grid; $b_t$ is the amount of power bought from main grid at a rate of $U_t^{rate}$: Lastly, $CU_i$ and $CD_i$ are the cost of starting up and shutting down each diesel unit. The second objective function (16) minimizes the $CO_2$ emissions from the diesel units. In (16), $EI_i$ and $ES_i$ are the intercept and slope of the emissions function, respectively.

$$\sum_{l=1}^{L} F_{lt} - x_{lt} + \sum_{j=1}^{J} sc_{jt} = \sum_{i=1}^{I} \sum_{k=1}^{K} g_{it}^k + \sum_{j=1}^{J} sd_{jt} + PV_t + b_t \qquad \forall t \tag{17}$$

Power Balance: Constraint (17) ensures total power supplied by the DERs always satisfies the current total load demand. It considers the power provided by the diesel units, the photovoltaic cells, and the collective discharge from the storage units along with the power bought from the main grid as the overall energy supply. The energy supply should satisfy the total forecasted load demand from all the busses (demand points) after load shedding and collective power to charge the storage units. In (17), $F_{lt}$ is the forecasted load demand and $PV_t$ is the power produced by the solar generators. The state of charge $s_{jt}$ is denoted with auxiliary variables reflecting charge $sc_{jt}$ and

discharge $sd_{jt}$. Although (17) is typically modeled as an equality constraint, where the resulting decisions ignore sudden power imbalances, additional power may be absorbed or injected into the MG to regulate power mismatch and rectify significant deviations.

$$g_{it}^k \leq GR_i^{k+1} u_{it}^k \qquad \forall i,t,k \geq \qquad (18)$$

$$\sum_{k=1}^{K} g_{it}^k - GR_i^{k+1} \leq M u_{it}^{k+1} \qquad \forall i,t,k \geq 1 \qquad (19)$$

$$u_{it}^{k+1} \leq u_{it}^k \qquad k \geq 1 \qquad (20)$$

Emission Segments: Although $CO_2$ emission from diesel units is a non-linear polynomial function; (16) can be linearized into segments based on the diesel unit power output. In this study, the linearized form of (16) includes two segments; (18)-(20) ensures no value is assigned to the second segment until the first segment is fulfilled. In (18), $GR_i^{k+1}$ refers to the operating segment along the emissions function which is linked to the diesel power output and subsequently the total operational cost. Note $M$ is simply a big number greater than the capacity of the total MG for segments to be mutually exclusive.

$$PG_i^{min} \leq \sum_{k=1}^{K} g_{it}^k \leq PG_i^{max} u_{it}^k \qquad \forall i,t \qquad (21)$$

$$-RD_i \leq \sum_{k=1}^{K} (g_{it}^k - g_{it-1}^k) \leq RU_i \qquad \forall i,t \qquad (22)$$

Diesel Units: Constraint (21) models diesel power limits denoted by $PG_i^{min}$ and $PG_i^{min}$ respectively, ensuring that only committed units can generate power. Similarly, (22) ensures the electricity from diesel units satisfy the up and down ramping limits denoted by $RD_i$ and $RU_i$.

$$s_{jt} = s_{jt+1} - \frac{sd_{jt}}{\mu_j} + \mu_j sc_{jt} \qquad \forall j,t > 1 \qquad (23)$$

$$M(1 - c_{jt}) \geq sd_{jt} \qquad \forall j,t \qquad (24)$$

$$Mc_{jt} \geq sc_{jt} \qquad \forall j,t \qquad (25)$$

$$SOC_j^{min} \leq s_{jt} \leq SOC_j^{max} \qquad \forall j,t \qquad (26)$$

Storage Units: In (23), the state of charge (SOC) considers the round-trip efficiency $\mu_j$ when charging and discharging. Charging is modeled as energy demand in the power balance constraint (17), whereas discharging is considered an energy supply. In the FED model, we assume that the storage units are full at the beginning of the planning horizon $t = 0$ and must be full at the end of the planning horizon $t = T$. The constraint set (24)-(25) ensures storage units cannot charge and discharge simultaneously using the binary indicator $c_{jt}$ and (26) enforces the upper and lower limits on the SOC denoted by $SOC_j^{min}$ and $SOC_j^{max}$ respectively.

$$x_{lt} \leq a F_{lt} \qquad \forall l,t \qquad (27)$$

$$\sum_{t=1}^{24} x_{lt} \leq b \sum_{t=1}^{24} F_{lt} \qquad \forall l \qquad (28)$$

$$U^{min} \leq b_t \leq U^{max} v_t \qquad \forall t \qquad (29)$$

$$v_t \leq b_t \qquad \forall t \qquad (30)$$

Load Shedding and Main Grid: The FED model uses an incentive-based DSM program attempting to decrease the energy consumption during the peak hours; however, the energy providers must reimburse the interruption costs in (15) to the consumers, incentivizing their participation in this

program. Constraint set (27)-(28) models a flexible load shedding program where the maximum amount of load demand that can be shed at each bus is regulated by the hourly percentage $a$ and daily percentage $b$. Constraint (29) shows the upper and lower limits of power that can be bought from the main grid. The proposed FED model is grid-connected and (30) indicates power exchange with the main grid.

$$RoCoF_{tn} = \frac{\left[ \begin{array}{c} \sum_{i=1}^{I} \sum_{k=1}^{2} (\Delta g_{itn}^{k}) \\ + \sum_{j=1}^{J} (\Delta sd_{jtn}) - D\Delta f_{tn-1} - b_t \end{array} \right]}{2H_t} \qquad \forall\, t > 1 \qquad (31)$$

$$rf^{min} \leq RoCoF_{tn} \leq rf^{max} \qquad\qquad \forall t \qquad (32)$$
$$\Delta f_{tn} = \Delta f_{tn-1} + RoCoF_{tn} * \tau \qquad\qquad \forall t \qquad (33)$$
$$f^{min} \leq \Delta f_{tn} \leq f^{max} \qquad\qquad \forall t \qquad (34)$$
$$H_t = \frac{\left[ \sum_{i}^{I} h_i * PG_i^{max} + \sum_{j}^{J} h_j * SOC_j^{max} \right]}{f^{nom}} \qquad\qquad \forall t \qquad (35)$$

Frequency Regulation: The rate of change of frequency (RoCoF) is formulated based on the swing equation which governs its dynamics [36]. In (31), $\Delta f_{tn}$ is the amount of deviation in frequency experience during the transition between grid-connected and islanded mode; $H_t$ is the MG inertia and $D$ is simply the load damping factor. Since there are no variations in power from diesel units, storage units, or frequency initially, we assume $RoCoF_{tn} = -b_t / 2H_t$ at $t = 0$. Constraint (32) ensures the post-fault RoCoF remain within its limits denoted by $rf^{min}$ and $rf^{max}$ while (33) calculates the frequency deviation, where $\tau$ is a sub-unit of time $t$ for sampling the deviations. (34) ensures that it remains within acceptable limits denoted by $f^{min}$ and $f^{max}$ to avoid load shedding or tripping protection relays. The MG inertia is calculated according to (35) to track grid stability where $h_i$ and $h_j$ are the inertial constant for diesel and storage units, respectively. The MG inertia is also a function of the nominal MG frequency $f^{nom}$, which varies across networks according to electrical codes.

## 4.2 Decision Criterion

The epsilon constraint method first proposed by [37] was used to solve the multi-objectivity. This method introduces an objective from a multi-objective problem as a constraint into a single objective problem. The unselected, primary objective is solved for a series of sub-problems as the selected, secondary constraint is tightened. Thus, the Pareto frontier for each significant state in the state space is generated. The knee solution from [38] was used as decision criteria to select the best-compromise solution along the Pareto Frontier for each significant scenario. In this study, emission was given priority over cost when selecting the best-compromise. Both the state space and the solution space were merged to form a training set for the NN's offline development.

## 5 RESULTS & DISCUSSION

Each module within the proposed framework was tested for its contribution to the overall MG tertiary control scheme. The historical data is climate sensor data retrieved from [28] and contains 9,384 hourly observations from June 2019 to July 2020. The proposed framework was applied to both the IEEE 18-bus and IEEE 33-bus networks to assess the scalability across different MGs. Both networks have a radial topology where the DERs are located at the reference bus near the loads, and their storage units have a round-trip efficiency of 0.95. The SSS algorithm and the NN were coded in Python while the proposed dispatch model was coded in AMPL and solved with CPLEX 12.1. All simulations ran on a computer with an Intel i7 2.67 GHz processor and 16 GB

RAM for replicability purposes. The attributes for the solar and wind power signal described in (3)-(14) were obtained from [39], and are outlined in Table 4 of the Appendix (Section A).

## 5.1 State Estimation

The climate factors used to approximate parameters of the dispatch model include the ambient temperature, solar irradiance, and wind speed. The raw data, box plot configuration was used within the proposed SSS algorithm to select the levels for each factor, and subsequently the bounds of integration for each factor's PDF. The levels within each factor and likelihood for each level to be used for determining the total number of treatments is summarized in Table 5.

Table 5: Design template using the raw data box plot configuration.

| Factor | Sensor Type / Model | Level | Quartile | Bounds | Probability |
|---|---|---|---|---|---|
| ambient temperature | Bandgap Campbell Scientific CS215 | 1 | Min - LW | [39.41, 61.25] | 0.0154 |
| | | 2 | LW - Q1 | [61.25, 73.95] | 0.3016 |
| | | 3 | Q1 - Q3 | [73.95, 82.44] | 0.4251 |
| | | 4 | Q3 - Max | [82.44, 94.3] | 0.2448 |
| solar irradiance | Silicon Photovoltaic Campbell Scientific CS215 | 1 | Q1 - Q3 | [0, 371.1] | 0.999 |
| | | 2 | Q3 - UW | [371.1, 927.5] | $10*e^{-16}$ |
| | | 3 | UW - Max | [927.5, 1126.25] | $10*e^{-16}$ |
| wind speed | Ultrasonic Vaisala 425A | 1 | Min - Q1 | [0.44, 2.7] | $10*e^{-16}$ |
| | | 2 | Q1 - Q3 | [2.7, 7.64] | 0.184 |
| | | 3 | Q3 - UW | [7.64, 15] | 0.782 |
| | | 4 | UW - Max | [15, 20.23] | 0.03 |

This design template is expanded in Table 10 of the Appendix (Section B) according to a traditional full factorial design. A diverse set of states with a significant probability of being observed throughout the solution space is described in Table 5.

Table 6: Scenarios derived from the SSS algorithm.

| Scenario | Ambient Temperature | Solar Irradiance | Wind Speed | Probability | Representative Date |
|---|---|---|---|---|---|
| 4 | 2 | 1 | 4 | 0.009 | 3/8/2020 |
| 7 | 3 | 1 | 3 | 0.332 | 9/2/2019 |
| 11 | 1 | 1 | 2 | 0.003 | 11/17/2019 |
| 14 | 1 | 1 | 3 | 0.012 | 1/21/2020 |
| 15 | 2 | 1 | 2 | 0.056 | 12/23/2019 |
| 16 | 4 | 1 | 4 | 0.007 | 9/21/2019 |
| 18 | 2 | 1 | 3 | 0.237 | 12/20/2019 |
| 31 | 3 | 1 | 4 | 0.013 | 5/14/2020 |
| 32 | 4 | 1 | 2 | 0.045 | 6/7/2020 |
| 38 | 4 | 1 | 3 | 0.191 | 6/6/2020 |
| 39 | 3 | 1 | 2 | 0.078 | 10/7/2019 |

In Table 6, the most frequently observed states throughout the year can be identified according to their joint probability. The dataset was filtered for each day that matched a scenario's condition for longest period throughout the state space. These days were selected as the best representative days for their respective scenarios. The chance of observing all scenarios described in Table 6 throughout is roughly 98%. Thus, these scenarios sufficiently represent the state space of the climate behavior and have a 98% chance to be experienced by the MG system throughout the year. The residual 2%

of the state space remains uncertain due to outliers and a lack of data to support those states. After verifying the proposed SSS algorithm has isolated significant scenarios, a reduction in model's complexity is consequently observed. This improves the speed of each subsequent module within the proposed framework. The total number of scenarios is calculated using the treatment combination of an experimental design, where $Level^{Factor} = Possible\ Scenarios = 4^2 \times 3^1 = 48$. After excluding unlikely scenarios using $P(factor \mid level\ x) < \alpha$ where $\alpha = 0.1\%$, only 11 of the 48 scenarios are considered significant for representing the state space. Thus, there is a 77% reduction in the number of scenarios which is directly proportional to a model's complexity. This is a drastic reduction in the models' complexity and consequently limits the number of resulting solutions while preserving most of the state space's information. Moreover, this reduction should improve the model's performance concerning speed while maintaining a comparable level of accuracy.

In this study, we chose the top three most dominant states throughout the collection period to model for MG resiliency. September 2$^{nd}$ 2019 is among the chosen states, dominating roughly a third of the year and there was a significant climate event occurring near Florida [28], where the data for this study was collected. During this time, [40] describes how Hurricane Dorian devastated the Bahamas. This level 5 system stagnated over Grand Bahama, near the Florida border. Thus, we chose to model these states and optimize the MG dispatch decisions for resiliency to extreme climate events.

## 5.2    Scaling Traditional Solutions

The bus characteristics for the IEEE-18 and IEEE-33 networks were obtained from [41], and outlined in Table 7 of the Appendix (Section A). In Table 7, $R_i$ denotes the ramp rate for each respective diesel unit. The data form Table 4, Table 7 and (1)-(14) are fed to the dispatch policy to obtain an exact solution for the dominant states in Table 6. The best-compromise solution along the Pareto frontier of each state was determined using the knee solution method [37]. The dispatch decisions denoting the solution space were combined with the state space to synthesize a dataset for the NN. Thus, the neural network was trained using the dataset described in Table 8.

Table 8: State and solution space combined into a dataset to train the NN.

| MG Feature | Type | No. of Units | | Description / Values |
|---|---|---|---|---|
| | | IEEE-18 | IEEE-33 | |
| Bus Count | Nominal | - | - | MG size. Values: 'IEEE-18', 'IEEE-33' |
| Wind Power | Numeric | 1 | 1 | Power (kWh) procured from wind speed |
| Solar Power | Numeric | 1 | 1 | Power (kWh) procured from solar irradiance |
| Demand | Numeric | 18 | 33 | Power (kWh) sold to consumers |
| Market Price | Numeric | 1 | 1 | Market value of power (kWh) in cents |
| Diesel | Numeric | 4 | 6 | Power (kWh) from diesel generators |
| Charge | Numeric | 6 | 6 | Power (kWh) absorbed by storage units |
| Discharge | Numeric | 6 | 6 | Power (kWh) released by storage units |
| Load Shed | Numeric | 18 | 33 | Power (kWh) not sold to consumers |
| Utility | Numeric | 1 | 1 | Power (kWh) purchased from the main grid |
| Frequency | Numeric | 2 | 2 | MG rate of change of frequency (+/-) attributes |

The dispatch policy parameters or input features for machine learning are [Bus Count, Wind Power, Solar Power, Demand, and Market Price]. Likewise, the decision variables or target vectors are

[Diesel, Charge, Discharge, Load Shed, Utility, and Frequency]. Notably, a MG feature can be decomposed into multiple attributes based on the size of the MG and the number of resources within that class of generators. For example, there are 18 demand nodes and 4 diesel generators within the IEEE-18 network. Thus, each node and generation unit are treated as an independent input vector for training purposes. However, a single vector is used to denote a single generator or aggregated data applicable to the entire MG such the net power imported from the main utility grid or the MG's nominal frequency.

## 5.3    Neural Network Performance for MG Dispatch

The dimensions of the dataset determine the initial configuration for the NN. The proposed NN architecture begins at a depth of one hidden layer and at a width of n + 1 neurons, where n is the length of the input vector. The depth and width can be adjusted after observing the initial learning behavior. The output layer has a length of m according to the length of the output vector. NNs have hyper parameters that affect their learning behavior. These hyper parameters of the initial configuration were optimized via grid search to improve the performance. The hyper parameters used for IEEE-18 and IEEE-33 networks are outlined in Table 9 of the Appendix (Section A).

The NN's architecture and complexity vary according to the number of resources in each MG and the variation of their output. Since the neurons are directly proportional to the size of the network, the IEEE33-NN is more complex than the IEEE18-NN. The rectifier (ReLU) activation function was used in all layers except the output layer. The vanishing gradient dilemma causes the network to have many neurons that fail to participate in the learning process and is a particular issue for MG systems. Many MG systems use DSM policies to regulate power exchange imbalances with load shedding, but load shedding is often the last resort among these polices and introduces many uninformative attributes to the dataset.  The ReLU activation function was chosen because it suffers least from vanishing gradient issues and offers flexibility to our network's output without overfitting. The Softplus activation function was used for on output layer because our target values are all non-negative, since the positive and negative RoCoF was decomposed into separate attributes.

During post-processing of the dataset, the output data points were observed falling between short intervals across all dimensions which imply a lack of outliers. Since there are few significant outliers, it is appropriate to calculate error based on the geometric distance between the predicted vector and target vector. The loss function chosen for the IEEE18-NN was the mean absolute error (MAE), defined in (36).

$$MAE = \frac{\sum_{i=1}^{n}|y_i - \hat{y}_i|}{n} \tag{36}$$

Unlike the IEEE-18 network, the output from DERs could vary by several orders of magnitude. Consequently, the range of values for a point within an individual attribute of the IEEE-33 dataset was larger than that of the IEEE-18 dataset. Thus, the loss function chosen for the IEEE33-NN was the mean square logarithmic error (MSLE) defined in (37).

$$MSLE = \frac{1}{N}\sum_{i-0}^{N}(\log(y_i + 1) - \log(\hat{y} + 1)^2 \tag{37}$$

The MSLE is used to normalize the contribution across all dimensions of the dataset and regulate the error associated with the geometric distance. Small errors in one dimension may be immense in another. The loss function for both the IEEE18-NN and IEEE33-NN are illustrated in Figure 4.
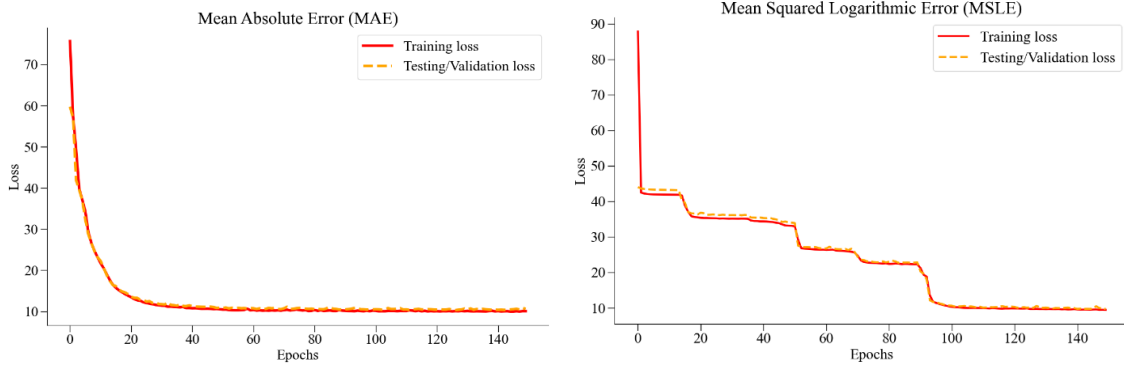


**Figure 4:** NN performance for the IEEE-18 (left) and the IEEE-33(right)

Figure 4 shows the total error calculated in the validation set over time. There was a vanishing gradient effect observed in epochs 20-60 in Figure 4b, which was corrected by the abrupt descent and immediate convergence. Increasing the learning rate shortened the time where the gradient disappeared, but simultaneously caused a reduction in learning stability. The graph here shows smooth loss curves over time without large oscillations, indicating stable learning.

To visualize the expressive power of the neural network after training is complete, we forward-propagate the validation set through the network to obtain its predictions and compare them to the target values. The prediction and target values for IEEE-18 and IEEE-33 networks can be visualized in Figure 5.
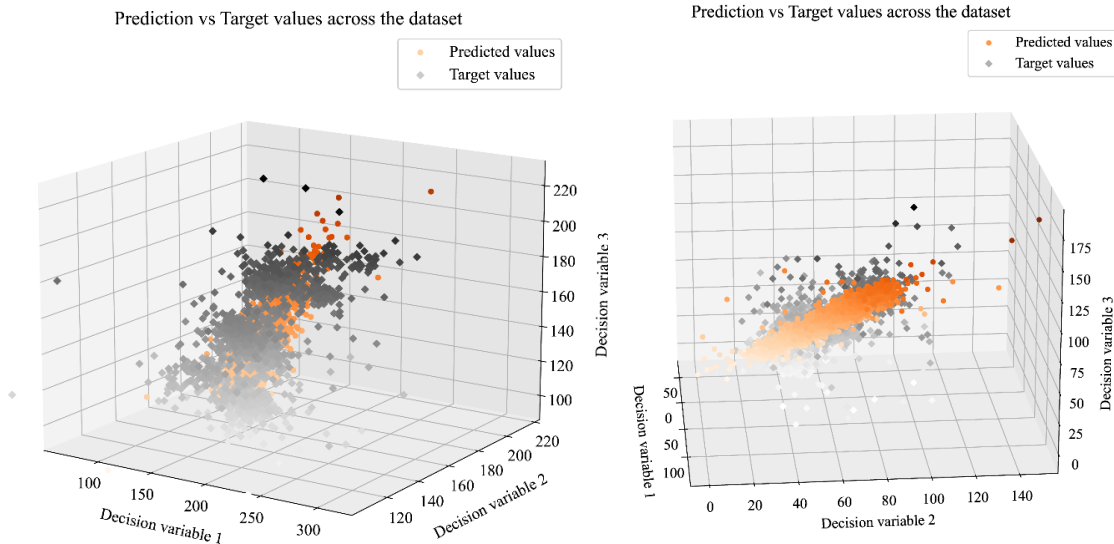


**Figure 5:** Predictive performance for the IEEE-18 (left) and IEEE-33 (right)

Since the values are high dimensional vectors previously described in Table 8, we extract three specific output dimensions according to their range and plot them as a three-dimensional cluster. Priority was assigned in this manner because diverse values will convey more information about the

network's performance. The topology of the individual clusters verified neither network was overfitting since the predicted values captured the region with the highest density of target values across both networks. The proposed NN takes roughly 5s to train on average for both MGs when compared to [29] and [36] which were solved using CPLEX in 110s and 37s respectively. Thus, the NN module can be applied to the test networks given the short time it takes to re-train the model. Moreover, the proposed framework and SSS algorithm can be applied to any physical system.

## 6  CONCLUSION

A modular design strategy for MG dispatch was presented in this study. The proposed framework synthesized dimension reduction, traditional dispatch policies, and modern machine learning. The proposed SSS algorithm limits the combinatorial expansion of treatments in a full factorial design to derive the state space of a MG system. SSS reduces the state space by nearly 77% while preserving roughly 98% of the original data and isolating the most dominant scenarios according to $\alpha$. Moreover, SSS highlights the most dominant states throughout the state space to identify extreme climate events experienced by the MG system. An existing dispatch policy was extended to consider carbon emissions and frequency regulation. The modified, multi-objective dispatch policy was used to obtain an exact solution for each state, where the best-compromise solution along the Pareto frontier was chosen according to the prioritized objective. The state space derived from the SSS algorithm and the solution space derived from the modified dispatch policy were synthesized into datasets to train the respective NN for each MG. The rectifier activation function was used to mitigate the vanishing gradient effect of DSM practices in MG dispatch such as load shedding. The output variations from the DERs influenced the dataset used for each MG. Thus, the MSLE was used for the IEEE-33 network instead of the MAE for the IEEE-18 network. Although the vanishing gradient effect was observed in Figure 5b, it was immediately corrected and the learning remained stable.

The proposed approach balances speed and scalability better than previous solution methods, but each module within the proposed framework should be enhanced to improve its overall utility. In future work, the dispatch model will include more MG system components, the fault detection module will be able to discern between sensor failure versus a system intrusion and the NN will be coupled with reinforcement learning.

APPENDIX A

Table 4: Solar panels and wind turbines attributes.

| Renewable | Attribute | Value |
|---|---|---|
| Solar Panels | Open circuit voltage | 21.98 V |
| | Short circuit voltage | 5.32 A |
| | Voltage temperature coefficient | 14.4 mV/$^{o}$C |
| | Current temperature coefficient | 1.22 mA/$^{o}$C |
| | Nominal cell operating temperature | 43 $^{o}$C |
| | Fill factor | 0.17 |

| | | Wind turbine capacity | 3000 kW |
|---|---|---|---|
| Wind Turbines | | Cut-in speed | 4 m/s |
| | | Cut-out speed | 25 m/s |
| | | Rated speed | 16 m/s |

Table 7: Diesel unit parameters from the IEEE-18 and IEEE-33 test networks.

| MG | Unit No. | $PG_i^{max}$ | $PG_i^{min}$ | $CU_i$ | $CD_i$ | $R_i$ | $EI_i$ | $CI_i$ | $CS_i$ |
|---|---|---|---|---|---|---|---|---|---|
| IEEE-18 | Gen 1 | 333.2 | 33.24 | 166.2 | 66.5 | 33.2 | 0.88 | 40 | 3.6 |
| | Gen 2 | 140 | 23.33 | 70 | 28 | 14 | 0.66 | 40 | 3.15 |
| | Gen 3 | 100 | 16.67 | 50 | 20 | 10 | 0.66 | 25 | 3.69 |
| | Gen 4 | 100 | 16.67 | 50 | 20 | 10 | 0.76 | 20 | 4.05 |
| IEEE-33 | Gen 1 | 80 | 8 | 40 | 16 | 8 | 0.88 | 40 | 3.6 |
| | Gen 2 | 80 | 8 | 40 | 16 | 8 | 0.66 | 48 | 3.15 |
| | Gen 3 | 50 | 5 | 25 | 10 | 5 | 0.66 | 25 | 3.85 |
| | Gen 4 | 55 | 5.5 | 27.5 | 11 | 5.5 | 0.764 | 28 | 3.76 |
| | Gen 5 | 30 | 3 | 15 | 6 | 3 | 1.02 | 15 | 4.15 |
| | Gen 6 | 40 | 4 | 20 | 8 | 4 | 0.764 | 20 | 4 |

Table 9: Hyper parameters used to configure the NN in the IEEE-18 and IEEE-33 test networks.

| Hyper Parameters | IEEE18-NN | IEEE33-NN |
|---|---|---|
| Batch size | 32 | 32 |
| Epochs | 150 | 150 |
| Learning rate | 0.007 | 0.007 |
| Optimizer | Adam | Adam |
| Activation Function | ReLU | ReLU |
| Loss Function | Mean Absolute Error | Mean Square Logarithmic Error |

APPENDIX B

Table 10: Scenarios derived from the SSS algorithm.

| Scenario | Ambient Temperature | Solar Irradiance | Wind Speed | Probability | Representative Date |
|---|---|---|---|---|---|
| 1 | 3 | 3 | 4 | - | - |
| 2 | 3 | 2 | 3 | - | - |
| 3 | 1 | 1 | 1 | - | - |
| 4 | 2 | 1 | 4 | 0.009048 | 3/8/2020 |
| 5 | 3 | 3 | 2 | - | - |
| 6 | 1 | 2 | 2 | - | - |
| 7 | 3 | 1 | 3 | 0.3324282 | 9/2/2019 |
| 8 | 1 | 3 | 1 | - | - |
| 9 | 2 | 1 | 1 | - | - |
| 10 | 2 | 2 | 1 | - | - |
| 11 | 1 | 1 | 2 | 0.0028336 | 11/17/2019 |
| 12 | 1 | 2 | 1 | - | - |
| 13 | 4 | 3 | 4 | - | - |
| 14 | 1 | 1 | 3 | 0.0120428 | 1/21/2020 |
| 15 | 2 | 1 | 2 | 0.0554944 | 12/23/2019 |
| 16 | 4 | 1 | 4 | 0.007344 | 9/21/2019 |

| 17 | 4 | 1 | 1 | - | - |
|---|---|---|---|---|---|
| 18 | 2 | 1 | 3 | 0.2358512 | 12/20/2019 |
| 19 | 2 | 3 | 2 | - | - |
| 20 | 2 | 2 | 4 | - | - |
| 21 | 1 | 2 | 4 | - | - |
| 22 | 4 | 3 | 3 | - | - |
| 23 | 1 | 3 | 3 | - | - |
| 24 | 1 | 3 | 2 | - | - |
| 25 | 4 | 2 | 1 | - | - |
| 26 | 3 | 2 | 4 | - | - |
| 27 | 4 | 3 | 1 | - | - |
| 28 | 3 | 3 | 3 | - | - |
| 29 | 2 | 3 | 3 | - | - |
| 30 | 1 | 2 | 3 | - | - |
| 31 | 3 | 1 | 4 | 0.012753 | 5/14/2020 |
| 32 | 4 | 1 | 2 | 0.0450432 | 6/7/2020 |
| 33 | 2 | 3 | 1 | - | - |
| 34 | 4 | 3 | 2 | - | - |
| 35 | 3 | 2 | 1 | - | - |
| 36 | 3 | 3 | 1 | - | - |
| 37 | 2 | 2 | 3 | - | - |
| 38 | 4 | 1 | 3 | 0.1914336 | 6/6/2020 |
| 39 | 3 | 1 | 2 | 0.0782184 | 10/7/2019 |
| 40 | 4 | 2 | 4 | - | - |
| 41 | 1 | 3 | 4 | - | - |
| 42 | 1 | 1 | 4 | - | - |
| 43 | 3 | 1 | 1 | - | - |
| 44 | 3 | 2 | 2 | - | - |
| 45 | 2 | 2 | 2 | - | - |
| 46 | 4 | 2 | 3 | - | - |
| 47 | 2 | 3 | 4 | - | - |
| 48 | 4 | 2 | 2 | - | - |

REFERENCES

[1] J. Zhao, E. Mazhari, N. Celik, and Y. J. Son, "Hybrid agent-based simulation for policy evaluation of solar power generation systems," *Simul. Model. Pract. Theory*, vol. 19, no. 10, pp. 2189–2205, 2011, doi: 10.1016/j.simpat.2011.07.005.

[2] P. Bartalos, Y. Wei, M. B. Blake, H. Damgacioglu, I. Saleh, and N. Celik, "Modeling energy-aware web services and application," *J. Netw. Comput. Appl.*, vol. 67, pp. 86–98, 2016, doi: 10.1016/j.jnca.2016.01.017.

[3] J. P. Sáenz, N. Celik, H. Xi, Y. J. Son, and S. Asfour, "Two-stage economic and environmental load dispatching framework using particle filtering," *Int. J. Electr. Power Energy Syst.*, vol. 48, no. 1, pp. 93–110, 2013, doi: 10.1016/j.ijepes.2012.11.009.

[4] A. Asadinejad, A. Rahimpour, K. Tomsovic, H. Qi, and C. fei Chen, "Evaluation of residential customer elasticity for incentive based demand response programs," *Electr. Power Syst. Res.*, vol. 158, pp. 26–36, 2018, doi: 10.1016/j.epsr.2017.12.017.

[5] Q. Shi, F. Li, Q. Hu, and Z. Wang, "Dynamic demand control for system frequency regulation: Concept review, algorithm comparison, and future vision," *Electr. Power Syst.*

*Res.*, vol. 154, pp. 75–87, 2018, doi: 10.1016/j.epsr.2017.07.021.

[6]     F. Darema, "Dynamic Data Driven Applications Systems: A New Paradigm for Application Simulations and Measurements," in *Proceedings of the 2004 International Conference on Computational Science*, 2004, pp. 662–669.

[7]     A. J. Aved, "Scene Understanding for Real Time Processing of Queries over Big Data Streaming Video," University of Central Florida, 2013.

[8]     D. Jin and D. M. Nicol, "Parallel simulation and virtual-machine-based emulation of software-defined networks," *ACM Trans. Model. Comput. Simul.*, vol. 26, no. 1, 2015, doi: 10.1145/2834116.

[9]     J. Xu, S. Zhang, E. Huang, C. H. Chen, L. H. Lee, and N. Celik, "MO2TOS: Multi-Fidelity Optimization with Ordinal Transformation and Optimal Sampling," *Asia-Pacific J. Oper. Res.*, vol. 33, no. 3, pp. 1–26, 2016, doi: 10.1142/S0217595916500172.

[10]    J. Xu, E. Huang, C. H. Chen, and L. H. Lee, "Simulation optimization: A review and exploration in the new era of cloud computing and big data," *Asia-Pacific J. Oper. Res.*, vol. 32, no. 3, pp. 1–34, 2015, doi: 10.1142/S0217595915500190.

[11]    M. Hunter, A. Biswas, and R. Fujimoto, "Energy efficient middleware for dynamic data driven application systems," *Proc. - Winter Simul. Conf.*, vol. 2018-Decem, pp. 628–639, 2019, doi: 10.1109/WSC.2018.8632433.

[12]    E. P. Blasch and A. J. Aved, "Dynamic data-driven application system (DDDAS) for video surveillance user support," *Procedia Comput. Sci.*, vol. 51, no. 1, pp. 2503–2517, 2015, doi: 10.1016/j.procs.2015.05.359.

[13]    E. Blasch, Y. Al-Nashif, and S. Hariri, "Static versus dynamic data information fusion analysis using DDDAS for cyber security trust," *Procedia Comput. Sci.*, vol. 29, pp. 1299–1313, 2014, doi: 10.1016/j.procs.2014.05.117.

[14]    X. Shi, H. Damgacioglu, and N. Celik, "A dynamic data-driven approach for operation planning of microgrids," *Procedia Comput. Sci.*, vol. 51, no. 1, pp. 2543–2552, 2015, doi: 10.1016/j.procs.2015.05.362.

[15]    E. Blasch, "DDDAS advantages from high-dimensional simulation," *Proc. - Winter Simul. Conf.*, vol. 2018-Decem, pp. 1418–1429, 2019, doi: 10.1109/WSC.2018.8632336.

[16]    M. Lecerf, D. Allaire, and K. Willcox, "Methodology for dynamic data-driven online flight capability estimation," *AIAA J.*, vol. 53, no. 10, pp. 3073–3087, 2015, doi: 10.2514/1.J053893.

[17]    X. Li, P. H. Tran, T. Liu, and C. Park, "Simulation-guided regression approach for estimating the size distribution of nanoparticles with dynamic light scattering data," *IISE Trans.*, vol. 49, no. 1, pp. 70–83, 2017, doi: 10.1080/0740817X.2016.1198063.

[18]    H. Damgacioglu, N. Celik, and A. Guller, "A route-based network simulation framework for airport ground system disruptions," *Comput. Ind. Eng.*, vol. 124, no. February, pp. 449–461, 2018, doi: 10.1016/j.cie.2018.07.029.

[19]    N. Sai Srinivas, N. Celik, Y. J. Son, and R. Lu, "Simulation-Based Aircraft Assembly Planning Using a Self-Guided Ant Colony Algorithm," in *Evolutionary Computing in Advanced Manufacturing*, 2011, pp. 169–195.

[20]    A. E. Thanos, X. Shi, J. P. Sáenz, and N. Celik, "A DDDAMS framework for real-time load dispatching in power networks," *Proc. 2013 Winter Simul. Conf. - Simul. Mak. Decis. a Complex World, WSC 2013*, pp. 1893–1904, 2013, doi: 10.1109/WSC.2013.6721569.

[21]    N. Celik, A. E. Thanos, and J. P. Saenz, "DDDAMS-based dispatch control in power networks," *Procedia Comput. Sci.*, vol. 18, pp. 1899–1908, 2013, doi: 10.1016/j.procs.2013.05.359.

[22]    M. Bastani, A. E. Thanos, H. Damgacioglu, N. Celik, and C. H. Chen, "An evolutionary simulation optimization framework for interruptible load management in the smart grid," *Sustain. Cities Soc.*, vol. 41, no. June, pp. 802–809, 2018, doi: 10.1016/j.scs.2018.06.007.

[23]    M. Bastani, T. Aristotelis E, N. Celik, and C. Chun-Hung, "EFFICIENT DESIGN SELECTION IN MICROGRID SIMULATIONS," in *Proceedings of the 2014 Winter Simulation Conference*, 2014, pp. 2762–2773, [Online]. Available: https://dl.acm.org/doi/10.5555/2693848.2694199.

[24]    J. Darville and C. Nurcin, "Microgrid Operational Planning using Deviation Clustering within a DDDAS Framework," in *International Conference on Dynamic Data Driven Application Systems*, 2020, pp. 77–84.

[25]    Z. Zhang, D. Zhang, and R. C. Qiu, "Deep reinforcement learning for power system: An overview," *CSEE J. Power Energy Syst.*, vol. 6, no. 1, pp. 213–225, 2019, doi: 10.17775/cseejpes.2019.00920.

[26]    H. Damgacioglu and N. Celik, "Integrated Optimization of Unit Commitment and Network Reconfiguration in Islanded AC Microgrids using a Two-stage Decomposition Method," *IEEE Trans. Power Syst.*, pp. 1–8.

[27]    G. Villarrubia, J. F. De Paz, P. Chamoso, and F. De la Prieta, "Artificial neural networks used in optimization problems," *Neurocomputing*, vol. 272, pp. 10–16, 2018, doi: 10.1016/j.neucom.2017.04.075.

[28]    "FAWN - Florida Automated Weather Network." https://fawn.ifas.ufl.edu/data/reports/ (accessed Dec. 01, 2020).

[29]    H. Damgacioglu, M. Bastani, and N. Celik, "A Dynamic Data-Driven Optimization Framework for Demand Side Management in Microgrids," *Handb. Dyn. Data Driven Appl. Syst.*, pp. 489–504, 2018, doi: 10.1007/978-3-319-95504-9_21.

[30]    M. H. Abokersh, M. Vallès, L. F. Cabeza, and D. Boer, "A framework for the optimal integration of solar assisted district heating in different urban sized communities: A robust machine learning approach incorporating global sensitivity analysis," *Appl. Energy*, vol. 267, no. April, p. 114903, 2020, doi: 10.1016/j.apenergy.2020.114903.

[31]    A. E. Thanos, M. Bastani, N. Celik, and C. Chen, "Framework for Automated Control in Microgrids," *IEEE Trans. Smart Grid*, vol. 8, no. 1, pp. 209–218, 2017.

[32]    D. C. Yu, T. C. Nguyen, and P. Haddawy, "Bayesian Network Model for Reliability Assessment of Power Systems," 1999.

[33]    "National Grid - Hourly Electric Supply Charges." https://www9.nationalgridus.com/niagaramohawk/business/rates/5_hour_charge.asp (accessed Jan. 29, 2020).

[34]    M. Wahbah, T. H. M. El-Fouly, B. Zahawi, and S. Feng, "Hybrid beta-KDE model for solar

irradiance probability density estimation," *IEEE Trans. Sustain. Energy*, vol. 11, no. 2, pp. 1110–1113, 2020, doi: 10.1109/TSTE.2019.2912706.

[35]   V. Sohoni, S. Gupta, and R. Nema, "A comparative analysis of wind speed probability distributions for wind power assessment of four sites," *Turkish J. Electr. Eng. Comput. Sci.*, vol. 24, no. 6, pp. 4724–4735, 2016, doi: 10.3906/elk-1412-207.

[36]   Y. Wen, C. Y. Chung, X. Liu, and L. Che, "Microgrid dispatch with frequency-aware islanding constraints," *IEEE Trans. Power Syst.*, vol. 34, no. 3, pp. 2465–2468, May 2019, doi: 10.1109/TPWRS.2019.2895573.

[37]   G. Mavrotas, "Effective implementation of the ε-constraint method in Multi-Objective Mathematical Programming problems," *Appl. Math. Comput.*, vol. 213, no. 2, pp. 455–465, 2009, doi: 10.1016/j.amc.2009.03.037.

[38]   A. Setämaa-Kärkkäinen, K. Miettinen, and J. Vuori, "Best compromise solution for a new multiobjective scheduling problem," *Comput. Oper. Res.*, vol. 33, no. 8, pp. 2353–2368, 2006, doi: 10.1016/j.cor.2005.02.006.

[39]   Y. M. Atwa, E. F. El-Saadany, M. M. Salama, and R. Seethapathy, "Optimal renewable resources mix for distribution system energy loss minimization," *IEEE Trans. Power Syst*, vol. 25, no. 1, pp. 360–370, 2010.

[40]   T. Cooper, "Hurricane Dorian," 2020. doi: 10.4324/9781003032311-20.

[41]   R. D. Zimmerman, C. E. Murillo-Sánchez, and R. J. Thomas, "MATPOWER: Steady-state operations, planning, and analysis tools for power systems research and education," *IEEE Trans. Power Syst.*, vol. 26, no. 1, pp. 12–19, Feb. 2011, doi: 10.1109/TPWRS.2010.2051168.